Effects of Varied Cosmic Ray Feedback from AGN on Massive Galaxy Properties

Charvi Goyal,[1] Sam B. Ponnada [ID],[1] Philip F. Hopkins [ID],[1] Sarah Wellons [ID],[2] Iryna S. Butsky [ID],[3, *]
Jose A. Benavides,[4] and FIRE Collaboration

[1]TAPIR, California Institute of Technology, Mailcode 350-17, Pasadena, CA 91125, USA
[2]Department of Astronomy, Van Vleck Observatory, Wesleyan University, 96 Foss Hill Drive, Middletown, CT 06459, USA
[3]Kavli Institute for Particle Astrophysics & Cosmology (KIPAC), Stanford University, Stanford, CA 94305, USA
[4]Department of Physics and Astronomy, University of California, Riverside, 900 University Avenue, Riverside, CA 92521, USA

ABSTRACT

Active galactic nuclei (AGN), provide energetic feedback necessary to 'turn off' star formation in high-mass galaxies ($M_{halo} \geq 10^{12.5}$ $M_\odot$, $10.4 \leq \log(\frac{M_*}{M_\odot}) \leq 11$) as observed. However, the physics that drives this "quenching" remains uncertain. Cosmic rays (CRs) have been proposed as a promising channel of AGN feedback, but the nature of CR-feedback from AGN requires further theoretical and observational constraints. Thus, we analyze a set of high-resolution simulations of massive galaxies from the Feedback in Realistic Environments (FIRE-3) project including multi-channel AGN feedback, explicitly evolving kinetic/mechanical, radiative, and spectrally-resolved CRs from the central black hole. Specifically, we explore different CR physics implementations and compare them to observed galaxy scaling relations. We find that all feedback parameterizations explored agree with observed galaxy scaling relations, demonstrating that varied CR injection efficiencies and locally-variable transport produce galaxies with reasonable bulk properties, but with orders-of-magnitude variant circumgalactic medium (CGM) gas properties. Our results indicate that detailed, multi-wavelength synthetic observations probing these varied simulated halo properties in conjunction with observational comparisons may place novel constraints on how AGN physically quench star formation in massive galaxies.

1. INTRODUCTION

The "quenching problem" of massive galaxies has been a longstanding discrepancy in galaxy formation between observed star formation rates and those predicted by simulations (Cole et al. 2002; Springel & Hernquist 2003; Longair 2008; Kereš et al. 2009; Benson 2010; Hopkins et al. 2023). Galaxies with high dark matter halo masses ($M_{halo} \gtrsim 10^{12.5}$ $M_\odot$) appear "red and dead" and are observed to have less gas cooling than predicted (Benson 2010). It is well-established that feedback processes play a vital role in preventing gas from cooling down and collapsing into stars (Longair 2008; Benson 2010; Hopkins et al. 2018), rectifying this 'overcooling problem; however, the specific mechanisms by which quenching occurs remain unclear.

Due to their immense mass and energy output, Active Galactic Nuclei (AGN) are thought to be critical suppressors of gas cooling in the interstellar medium (ISM), circum-galactic medium (CGM) and intracluster medium (ICM) (Longair 2008; Benson 2010; Somerville & Davé 2015; Su et al. 2021). Studies have found that models with AGN feedback channels are necessary to explain massive galaxy properties when compared to non-AGN counterparts (Harrison et al. 2018; Su et al. 2019a, 2021; Hopkins et al. 2023; Wellons et al. 2023), which is why most modern simulations which aim to reproduce the observed bulk properties of galaxies in a statistical manner include AGN feedback (Schaye et al. 2014; Sijacki et al. 2015; Somerville & Davé 2015; Davé et al. 2019).

How energy from AGN is transferred and coupled to the gas of the host galaxy is now the major open question. Motivated by observations, most of the theoretical literature has focused on the radiative and mechanical

feedback modes of AGN (see Harrison & Almeida 2024, for a recent review). Observed UV and X-ray emission from AGN suggest that AGN generate strong radiation fields due to accretion, which can Compton-heat and photo-ionize gas, as well as drive winds via radiation pressure. AGN have also been observed to drive non-radiative mechanical outflows from disk instabilities, in the forms of jets (Fabian 2012; Heckman & Best 2014), which can evacuate large bubble-like cavities and thermalize energy in surrounding gas via shocks and turbulent mixing.

Synchrotron emission observed from relativistic jets of AGN and observations of ultra-high energy cosmic rays (Berezinsky et al. 2006) have suggested that AGN may also produce cosmic rays (CRs), which could affect surrounding gas both by dissipating energy due to streaming instabilities and collisions (Bustard & Zweibel 2021), and by creating large-scale non-thermal pressure gradients in galactic halos (Butsky & Quinn 2018; Su et al. 2019b; Hopkins et al. 2020b). Which of these modes, or combination of them, can viably quench galaxies is a topic of ongoing study in galaxy formation (Benson 2010; Somerville & Davé 2015; Su et al. 2019b, 2021; Wellons et al. 2023; Byrne et al. 2024).

Recent progress in galaxy evolution simulations has allowed for higher hydrodynamic resolution and explicit modeling of different AGN feedback modes, most recently including CRs, along with their dynamical, thermo-chemical, and radiative couplings to gas (Hopkins et al. 2023). While some studies have found CRs to be a promising AGN feedback mechanism (Ruszkowski et al. 2017; Su et al. 2019b; Wellons et al. 2023), the details of CR production by AGN and how CRs feedback couples to the host galaxy and surroundings are largely unknown theoretically, and the plausible parameter space remains vast, retaining degeneracies even after detailed, multi-wavelength observational comparisons (Byrne et al. 2024; Ponnada et al. 2025b).

In this study, we explore the orders-of-magnitude variable parameter space of CR feedback from AGN and show that these models reasonably reproduce observed properties of high-mass galaxies ($M_{halo} \approx 10^{13}$ $M_{\odot}$), but crucially differ in their CGM properties, potentially allowing for constraints on these 'micro-physical' parameters via emergent observables. We use cosmological zoom-in, cosmic-ray-magneto-hydrodynamic (CR-MHD) galaxy formation simulations from the Feedback In Realistic Environments project (FIRE-3)[1] (Hopkins et al. 2023), which allows for a more advanced treatment

of CR and black hole physics. The relevant physical parameters we vary reflect the uncertainties in CR physics on small, unresolved scales (on the scales of CR gyro-radii, which are $\sim$AU in typical magnetic field strengths for GeV CRs) in terms of their transport (parameterized by prescriptions for the effective macroscopic scattering rate, which gives rise to diffusion- and streaming-like behaviors) and how efficiently CRs are produced by AGN, i.e., the percentage of AGN accretion energy that is output in the form of CRs. In Section 2, we describe our suite of simulations and analysis methodology before presenting our analysis of the simulations and their properties in Section 3. Finally, in Section 4, we discuss and conclude our findings.

2. METHODS

2.1. *Simulations*

We analyze a set of FIRE-3 cosmic-ray-magnetohydrodynamic (CR-MHD), cosmological zoom-in simulations, evolved with the GIZMO hydrodynamics solver in meshless-finite-mass mode (Hopkins 2015). All simulations include standard FIRE-3 physics and methods as detailed in Hopkins et al. (2023). We model star formation in high density ($\gtrsim 1000$ cm^{-3}), self-gravitating, Jeans-unstable gas with converging (or slowly diverging) flows with respect to the local free-fall timescale on resolved scales. Explicit stellar evolution follows up-to-date stellar evolution tracks, with feedback arising from radiation pressure, Type I and II supernovae, stellar winds from OB and AGB stars, photoionization, and photo-electric heating. Stellar feedback is fully coupled to multi-band (extreme UV to far infrared) radiation transport and gas cooling from 10^0 - 10^{10} K. This, in conjunction with high, adaptive numerical resolution ($M_{gas} \sim 3 \times 10^5$ $M_{\odot}$) naturally gives rise to a multi-phase interstellar and circumgalactic medium.

All simulations include magnetic fields and anisotropic transport and viscosity, using MHD methods described in Hopkins & Raives (2015) and Hopkins et al. (2016). The cosmic ray physics is coupled directly to the magnetohydrodynamics, with the full CR spectrum of MeV-TeV protons and electrons propagated along magnetic field lines according to the fully general CR transport equations, and interacting with the gas via scattering, Lorentz forces, and losses, as described in Hopkins et al. (2022a). CRs from SNe and fast stellar winds are injected with 10% of the initial SNe/wind kinetic energy and a power-law injection spectrum motivated by diffusive shock acceleration.

Our simulation suite consists of 4 sets of **m13** (in reference to their dark matter halo mass $M_{halo} \sim 10^{13}$ $M_{\odot}$) FIRE galaxies. The four m13 halos are h206 (some

Halo	Model	$\epsilon_{\mathrm{CR}}^{\mathrm{BH}}$ [10^{-4}]	$\log_{10}(\mathrm{M_{halo}})$ [$\mathrm{M_\odot}$]	$\log_{10}(\mathrm{M_*})$ [$\mathrm{M_\odot}$]
h206	CD	3	12.69	10.93
h206	VDLoCR	1	12.68	10.85
h206	VDMidCR	10	12.69	10.75
h206	VDHiCR	30	12.68	10.41
h113	CD	3	12.78	11.18
h113	VDMidCR	10	12.79	11.00
h236	CD	3	13.08	10.96
h236	VDMidCR	10	13.11	10.85
h029	CD	3	12.98	11.37
h029	VDMidCR	10	12.98	11.1

Table 1. Properties of the FIRE-3 simulation suite analyzed in this work. The columns, from left to right, are: name of the halo evolved in FIRE-3, the CR model used to evolve it, energy efficiency of CR injection by the AGN, halo mass, and stellar mass. 'VD' models have a variable diffusion coefficient derived from ISM properties whereas 'CD' models have a constant power-law diffusion coefficient. The prescription with which stellar and halo mass are defined is described in more detail in Section 2.2.

variations of which were explored in Byrne et al. 2024; Ponnada et al. 2025b), h113, h029, and h236. These simulations all include black holes (BHs) and their explicit associated radiative, mechanical, and cosmic ray feedback modes following Hopkins et al. 2023; we refer the reader to details therein regarding those feedback channels.

In brief, BH mechanical feedback utilizes a hyper-refined particle spawning method, with particles of ∼1000 times higher resolution (lower particle mass) initiated preferentially along the angular momentum axis of the BHs (as perfectly collimated jets) before de-refinement upon mixing into the surrounding gas cells via reaching the local sound speed. All simulations explored in this study utilize initial mechanical wind velocities of 3000 km s^{-1} and a radiative momentum flux coupling (L/c) of 1.

Each of the four halos was evolved with different CR physics models, varying the energy fraction of AGN accretion that is injected as CRs and the CR transport model. The energy fraction determines the rate of energy injected from the AGN into surrounding gas cells as CRs (with the same injection spectrum as from SNe) whenever mechanical energy is deposited as follows:

$$\dot{E}_{\mathrm{CR}}^{\mathrm{BH}} \equiv \epsilon_{\mathrm{CR}}^{\mathrm{BH}} \dot{M}_{\mathrm{BH}} c^2$$

where $\dot{E}_{\mathrm{CR}}^{\mathrm{BH}}$ is the CR injection energy rate, $\epsilon_{\mathrm{CR}}^{\mathrm{BH}}$ is the energy fraction, and $\dot{M}_{\mathrm{BH}}$ is the black hole accretion rate (Hopkins et al. 2023).

The two CR transport models we explore are: 1) a temporally and spatially constant power-law scattering rate, which gives rise to an effective diffusion coefficient as a function of CR rigidity (R) of $\kappa_{\mathrm{eff}} \sim \mathrm{R}^{0.6}$, hereafter referred to as 'CD', and 2) a variable diffusion coefficient dependent on the ISM properties, motivated by the "external driving" model as described in

(Hopkins et al. 2022b) to calibrate scattering rates to reproduce Voyager and AMS-02 observations in Milky Way-mass FIRE-3 simulations, hereafter referred to as 'VD'. The VD model is similar in principle to scattering models predicted by "extrinsic turbulence" models (Jokipii 1966), however, with the empirically-motivated addition of a turbulent driving term at gyro-resonant wave-numbers to reproduce the correct spectral shapes in Milky Way Solar Circle-like conditions. We pair the VD model with three CR injection efficiencies: 1×10^{-4} (low), 1×10^{-3} (medium), and 3×10^{-3} (high), hereafter referred to as 'VDLoCR', 'VDMidCR', and 'VDHiCR', respectively. We summarize the simulations analyzed in Table 1.

2.2. Derived Quantities

We calculate several bulk galaxy properties for each simulation, by the same prescriptions as Wellons et al. (2023) and Byrne et al. (2024). Halo mass is defined as the total mass inside R$_{200}$. The stellar mass is computed as the total mass of stars within 50 kpc of the galaxy's center, where the galaxy center is defined by the location of the central supermassive black hole (SMBH). For all snapshots, we orient the galaxies face-on using the angular momentum vector of the star particles to define the rotation axis, and transform all cell vector fields accordingly.

We then measure the 300-Myr averaged star formation rate (SFR) at $z = 0$ as the total mass of stars formed in the last 300 Myr within 50 kpc, averaged over that timescale. The effective radius, defined as the two-dimensional radius enclosing half of the stellar mass when the galaxy is viewed face-on, is used to calculate the velocity dispersion of stars, σ, which is defined as the standard deviation of the radial velocity of stars (the $\hat{z}$-component) within the effective radius.

2.3. *Radial Profiles and Time Series*

We also analyze various radial profiles for each simulation snapshot. The CR energy density profiles at different redshifts are computed as the total CR energy contained in shells of ~ 1.7 kpc thickness at a given radius away from the galaxy's center, divided by the volume of each shell. Following a similar procedure, we also generate gas number density and effective CR diffusion coefficient ($\kappa_{\rm eff}$) profiles for different redshifts. To calculate $\kappa_{\rm eff}$, we first average the diffusivity of the $\sim$.1-100 GeV proton spectrum by taking the energy-weighted mean of the diffusivities of the spectral bins for each given cell. Then, we use the aforementioned volume-weighting to obtain a radial profile of $\kappa_{\rm eff}$.

In addition to radial profiles, we calculate the CR injection rates from stellar sources and AGN for each run until $z = 0$. We first calculate the time-series SFR as the total mass of star particles formed within 50 kpc of the galactic center, corrected for mean mass loss rates to obtain the at-formation stellar mass (Hopkins et al. 2023). From there, we approximate the stellar CR injection rate as $\dot{E}_{\rm CR}^* \approx 0.1 \times 10^{51}$ erg $(\dot{M}_*/100 M_\odot)$, where 0.1×10^{51} erg is the amount of CR energy released from a single supernova event, which occurs approximately once per $100\,M_\odot$ of the stars formed. To obtain the cumulative CR energy injected into the galaxy by stellar feedback, we integrate the injection rate over time. We use the AGN accretion rate to calculate the CR injection rate from the AGN, where $\dot{E}_{\rm cr}^{\rm BH} \equiv \epsilon_{\rm cr}^{\rm BH} \dot{M}_{\rm BH} c^2 \approx 1.8 \times 10^{59}$ erg $(\dot{M}_{\rm BH}/10^8 M_\odot)(\epsilon_{\rm CR}^{\rm BH}/10^{-3})$. We cumulatively integrate the time-series injection rates over time for each source to find the cumulative CR energy injected into the galaxy by each source.

3. RESULTS

3.1. *Bulk Properties*

The bulk properties of the galaxies are plotted in Figure 3.1, and show that the models produce galaxies that are in agreement with known empirical scaling relations.

The top panel shows the stellar mass - halo mass (SMHM) relation, tracking the amount of star formation regulation. The galaxies are compared to the median observational SMHM found by Behroozi et al. (2019) of central galaxies (both star-forming and quenched), following Wellons et al. (2023), with galaxies within 0.5 dex of the line being considered as properly regulated. All models explored here produce galaxies that fall within the range of being well-regulated. As might be expected, higher cosmic-ray injection efficiency (stronger feedback) leads to increased regulation of the stellar mass. VD models produce more regulated galaxies in comparison to the CD model, including the VDLoCR
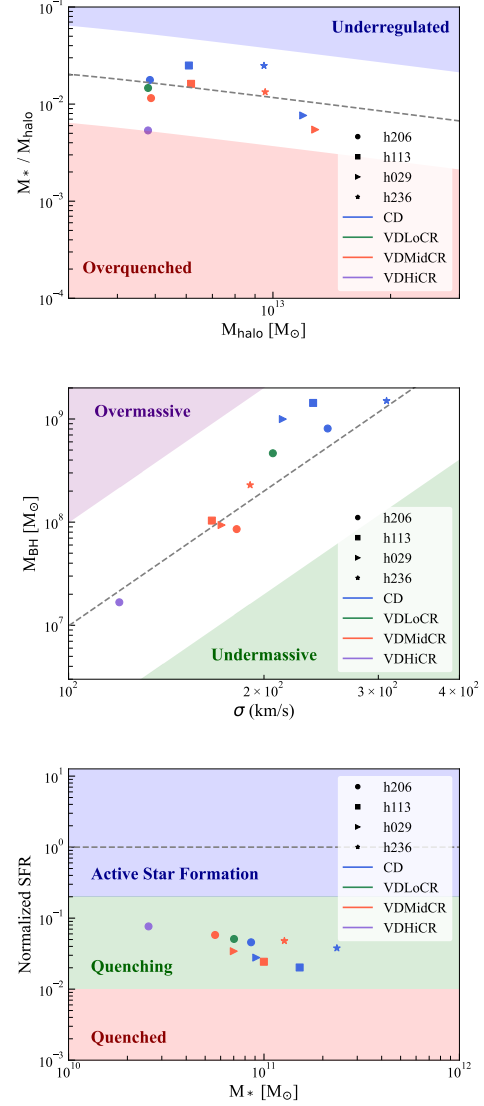

Figure 1. Scaling relations for all `h206`, `h113`, `h029`, and `h236` runs at $z = 0$, indicated by squares, circles, triangles, and stars, respectively. Blue, green, red, and purple markers indicate runs with the CD, VDLoCR, VDMidCR, and VDHiCR model, respectively. Irrespective of the details of CR physics, all models produce well-regulated, mildly quenched galaxies with reasonable SMBH masses, in agreement with the scaling relations. ***Top:*** The stellar mass - halo mass relation from Behroozi et al. (2019) (dashed line). The blue and red regions describes galaxies with under-regulated and overquenched stellar populations respectively. ***Center:*** The $M_{\rm BH}$-σ relation from Greene et al. (2020) (dashed line). The purple and green regions describes galaxies with overly-massive and undermassive AGN respectively. ***Bottom:*** The 300-Myr averaged star formation rate, normalized to the median value of star formation observed in star-forming galaxies at $z = 0$ from Salim et al. (2007). The blue, green, and red regions describe actively star forming, quenching, and quenched galaxies.
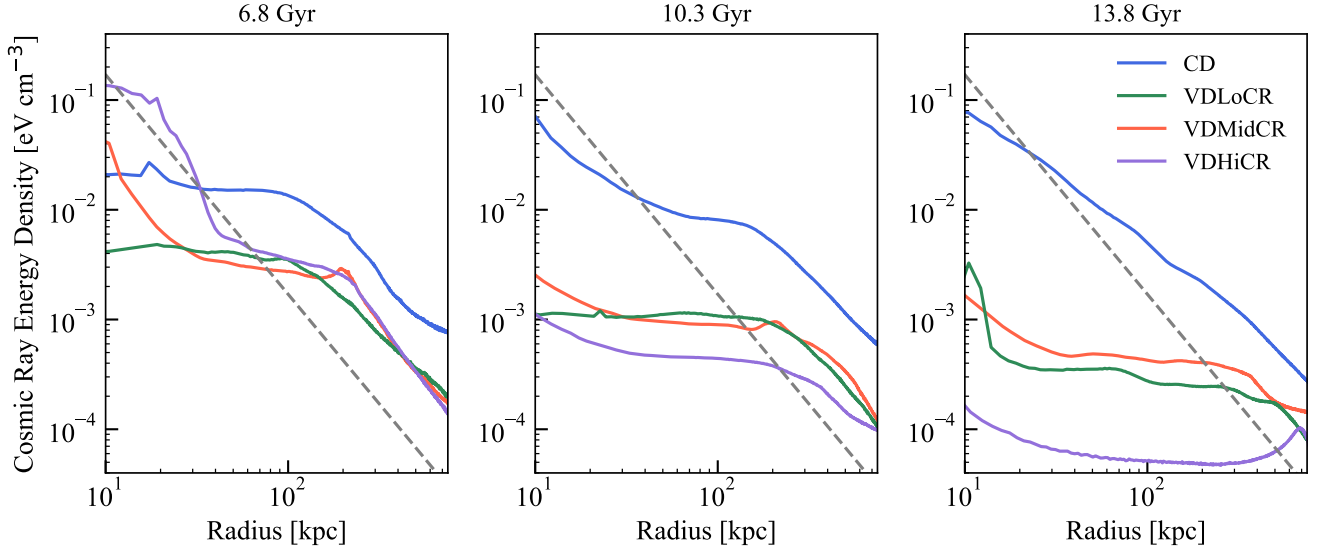
Figure 2. Radial profiles of the volume-weighted mean e_{CR} in the halos of the `h206` runs, binned in ~1.7 kpc spherical annuli. Snapshots at $\tau = 6.8, 10.3, 13.8$ Gyr are shown in the left, center, and right panels respectively. The gray dashed line is the $1/r^2$ profile expected from steady state CR injection and $\kappa_{eff} \propto r$ (Butsky et al. 2023). VD models have increasingly flatter profiles over time, with a nonlinear relationship between the normalization of the e_{CR} profiles and CR injection efficiencies (ϵ_{CR}^{BH}).

run of `h206`, despite having a lower CR injection efficiency than CD. We also note that M_{halo} has little variation across models for each halo, producing a qualitatively distinct vertical band for each halo in the panel. In the middle panel of Figure 3.1, we show the M_{BH}-σ relation at $z = 0$, where σ refers to the velocity dispersion of stars, as described in 2.2. The models are compared with the observational relation of Greene et al. (2020), with the model SMBH considered to be properly massive if the mass is within .5 dex of the observational constraint. All models we explore also follow this relation. Models with higher cosmic-ray injection efficiencies are seen producing galaxies with lower AGN mass and velocity dispersion, suggesting that the stronger the CR feedback, the more self-regulation of AGN growth, corresponding with the same trend as seen in the SMHM relation. However, the CD model produces galaxies with the highest black hole mass despite having higher CR efficiency than VDLoCR, suggesting that variable CR transport is better able to regulate AGN growth. The M_{BH}-σ relation also appears to be less sensitive to variations in initial halo conditions, producing a cluster for each specific model across different halos.

The bottom panel shows the 300-Myr averaged SFR of each model variation and halo at $z = 0$, normalized to the median star formation expected from a star forming main sequence galaxy (including AGN/SF composite galaxies) at $z = 0$ as found by Salim et al. (2007), against the stellar mass to measure star formation suppression.

All runs are within 1-2 dex below the expected SFR for actively star forming galaxies, indicating that the galaxies are mildly quenched. VD models appear to have marginally higher $z = 0$ SFRs but lower stellar masses than their CD counterparts for the same halo. Thus, we find that all CR parameterizations explored yield reasonably quenched galaxies with appropriate stellar and black hole masses at this halo mass scale.

3.2. *CGM Properties*

In this subsection, we present radial profiles of various physical quantities in the CGM from our simulations. We find that all halos produce similar qualitative profile trends for a given physics variation, so we focus on `h206` hereafter. The radial profiles of CR energy density are shown in Figure 2. Different models exhibit different radial profiles of CR energy density, or equivalently the CR pressure, as $P_{CR} \approx \frac{1}{3} e_{CR}$ for $\gamma_{CR} = 4/3$. In particular, CD and VD models evolve differently with time, with the CD model presenting a power-law-like profile at late times and VD models exhibiting qualitatively flatter radial profiles, particularly at late times. For the VD models of varied injection efficiency, we find that the CR energy density profiles in the CGM at $z = 0$ exhibit a nonlinear ordering, where the VDMidCR model has the highest e_{CR} amongst all VD models at radii $\gtrsim 15$ kpc. The VDHiCR model produces the largest variation in its e_{CR} profile over time, having the highest e_{CR} at earlier times (with $\tau = 6.8$ Gyr shown in Fig. 2) among the VD models and then decreasing to the lowest energy density
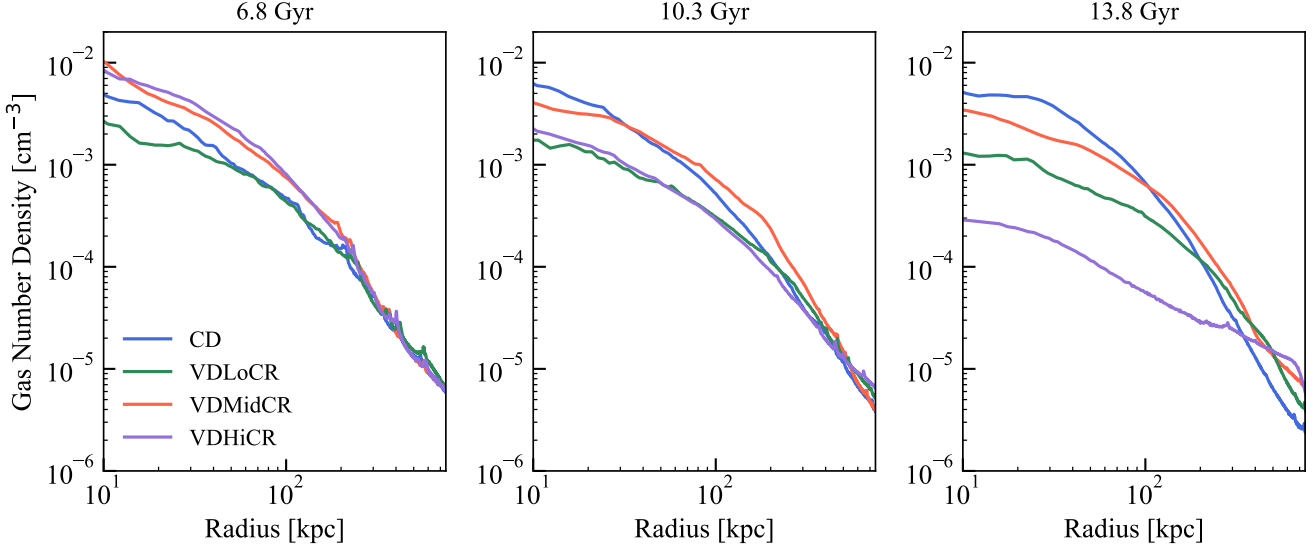
Figure 3. Radial profiles of the volume-weighted mean n_{gas} for the h206 runs, from 10 kpc to 750 kpc binned in ~1.7 kpc spherical annuli. Snapshots at $\tau = 6.8, 10.3, 13.8$ Gyr are shown in the left, center, and right panels respectively. Similar trends as the CR density profile suggest dynamical coupling of CRs to gas.

at $z = 0$, with its CGM e_{CR} nearly an order of magnitude lower at a given radius than that of VDMidCR and VDLoCR models at $z = 0$.

The VDHiCR model exhibits a similar trend over time in its radial profile of gas number density (Figure 3). At $z = 0$, the gas density radial profiles share the same ordering with CR injection efficiency as CR energy density does; in general, CGM gas density profiles appear to flatten over time irrespective of the model variation, particularly within $r \lesssim 300$ kpc (out to the approximate virial radii of these halos). The similarities between the CGM gas density and CR energy density owe to the dynamical coupling of CRs to the gas, as steep gradients in e_{CR} at the edge of flattened "shelves" in the profiles aid in outflows. Since the CRs can diffuse, and the CR pressure is time-dependent, the shelves in e_{CR} can move ahead of the gas (Hopkins et al. 2021; Ponnada 2025), and so e_{CR} as a function of radius (or gas density) does not appear to trace an exact, tightly-coupled adiabat (Hopkins et al. 2022a). Despite this caveat, and even though these halos are not CR pressure dominated overall, there appears to be some degree of spatial correspondence between the gradual flatteing of e_{CR} with time shown in Fig. 2 and the qualitative dilution and flattening of the gas density profiles with time in Figure 3, particularly in the VDHiCR case which has the largest modulation in AGN-injected e_{CR} over time.

In Figure 4, we show the radial profiles of the volume-weighted mean CR *effective* diffusion coefficient (which is itself energy-averaged over all CR energy bins for

each gas cell; see Section 2), κ_{eff}, at different redshifts. Here, κ_{eff} contains both 'diffusion-like' and 'streaming-like' terms which emerge from the evolved scattering rate as a function of rigidity, $\nu_{CR}(R)$, but *not* the advective transport of CRs. The CD model, as expected, has a largely constant effective diffusivity, with slight changes representing small shifts in the CR energy spectrum from the canonical $\sim$ GeV peak at a given radius. The "troughs" present in the VD profiles correspond to areas of lower diffusivity surrounded by high diffusivity that could trap CRs, thus creating e_{CR} overdensities. Indeed, we see such troughs in κ_{eff} correspond to overdensities in e_{CR} in Figures 2 and 4 e.g. in VDHiCR at $\sim$15 and $\sim$200 at $\tau = 6.8$ Gyr; in VDMidCR at $\sim$200 kpc at $\tau = 10.3$ Gyr and $\sim$400 kpc at $\tau = 13.8$ Gyr; and in VDLoCR at $\sim$15 kpc at $\tau = 10.3$ Gyr. Sharper troughs correspond to stronger local CR pressure gradients and overdensities.

3.3. *Cosmic Ray Injection Histories & Implications for Quenching*

Similarly to Byrne et al. (2024), we approximate the total energy of CRs produced from stars over the age of the universe as $E^*_{CR} \approx 0.1 \times 10^{51}$ erg $(M_{sf}/100 M_\odot)$, where 0.1×10^{51} erg is the amount of CR energy released from a single supernova event, which occurs approximately once per $100\,M_\odot$ of the stars formed, and M_{sf} is the cumulative at-formation stellar mass (see Section 2.3 for more detailed methodology). Similarly, we approximate the total CR energy produced by the AGN as $E^{BH}_{CR} = \epsilon^{BH}_{CR} M_{BH,acc} c^2 \approx 1.8 \times$
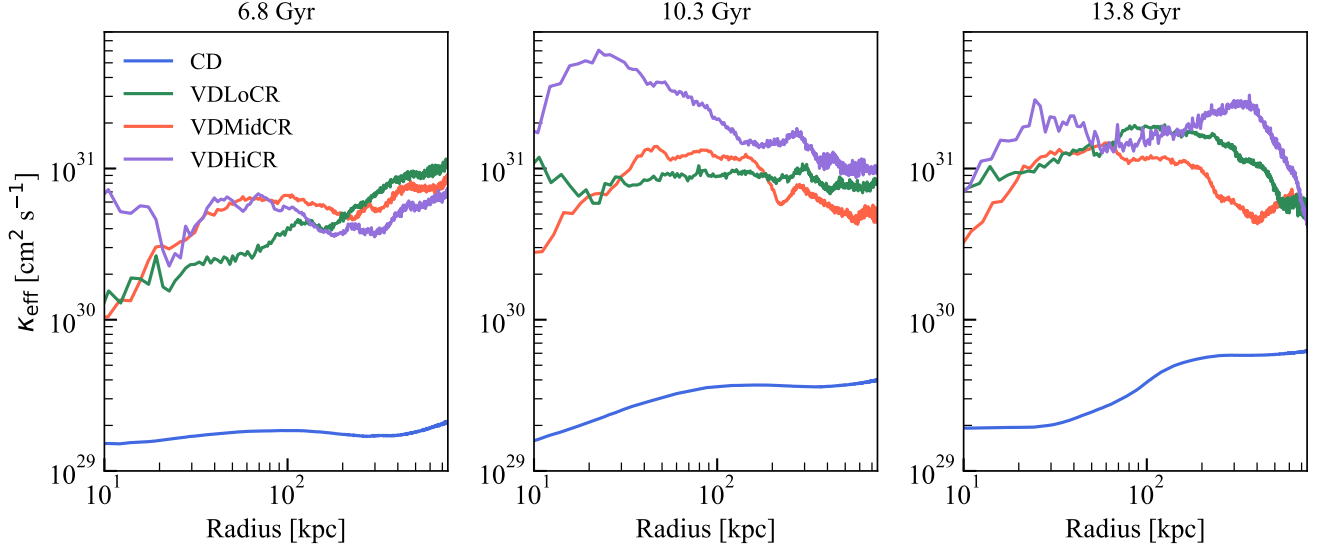
Figure 4. Radial profiles of the volume-weighted mean cosmic ray diffusivity κ_{eff} in the halos of the `h206` runs, from 10 kpc to 750 kpc binned in ~ 1.7 kpc annuli. Snapshots at $\tau = 6.8, 10.3, 13.8$ Gyr are shown in the left, center, and right panels respectively. The presences of troughs suggests the possibility of CR winds.

10^{59} erg $(M_{\mathrm{BH,acc}}/10^8 M_\odot)(\epsilon_{\mathrm{CR}}^{\mathrm{BH}}/10^{-3})$ where $M_{\mathrm{BH,acc}}$ is the cumulative mass accreted onto the AGN. Table 2 summarizes the cumulative CR energy deposited from each source by $z = 0$ for all runs in our simulation suite.

We find that while VD runs have at most ~ 1.6 times more CR energy from AGN feedback compared to stellar feedback, the CD runs have up to ~ 3.3 times the CR energy from AGN vs. stellar sources. The CD runs produce more CR energy from both stars and the AGN compared to VDMidCR across all halos, despite having a lower injection efficiency.

This suggests that not only does the VD transport model control AGN growth more effectively than CD, producing smaller ratios between $E_{\mathrm{CR}}^{\mathrm{BH}}$ and E_{CR}^*, but it also suppresses overall CR production in the galaxy. Moreover, this indicates that the primary way in which the increased CR feedback efficiency regulates galaxy growth is not via aggregate injection of CRs, but rather due to the *timing* of injection, which is inherently chaotic and sensitive to the 'responsiveness' of the BH feedback model, as described in Wellons et al. (2023).

Interestingly, we also find that while E_{CR}^* decreases linearly with CR injection efficiency in `h206`'s VD runs, $E_{\mathrm{CR}}^{\mathrm{BH}}$ peaks with VDMidCR, highlighting the same non-linear behavior of increasing CR feedback efficiency as seen in the CR energy density profiles in the CGM at $z = 0$ (Figure 2).

We calculate the CR injection rates from stellar and AGN feedback for the `h206` runs and present them in Figure 5. We find increasing variability in AGN injec-

Halo	Model	E_{cr}^* [10^{58} erg]	E_{cr}^{BH} [10^{58} erg]
`m13h206`	CD	10.74	33.22
`m13h206`	VDLoCR	8.78	4.94
`m13h206`	VDMidCR	7.03	7.12
`m13h206`	VDHiCR	3.21	5.15
`m13h113`	CD	19.03	63.28
`m13h113`	VDMidCR	12.48	9.99
`m13h236`	CD	11.42	38.2
`m13h236`	VDMidCR	8.76	13.31
`m13h029`	CD	29.5	27.95
`m13h029`	VDMidCR	15.9	16.28

Table 2. Approximate total CR energy produced in all `h206`, `h113`, `h029`, and `h236` runs until $z = 0$ from stellar and black hole sources. The columns, from left to right, are the name of the halo evolved in FIRE-3, the CR model used to evolve it, the total CR energy produced by stars, and the total CR energy produced by the AGN. VD runs have less CR production than their CD counterparts, and less AGN feedback relative to the amount of stellar feedback.

tion rates for VD models with increasing injection efficiency, indicating higher responsiveness of the feedback model. The CD model produces AGN injection rates systematically higher than those of VDLoCR after ~ 5 Gyr despite having similar profiles before then. Note again, the CD model has a factor of 3 higher CR injection efficiency than that of VDLoCR and a factor of ~ 6.7 larger total $\mathrm{E}_{\mathrm{CR}}^{BH}$ and despite this, the VDLoCR model exhibits stronger regulation on the scaling relations (Figure 3.1). This indicates that the CR transport variation alone can play a significant role in the responsiveness of a given AGN feedback model.
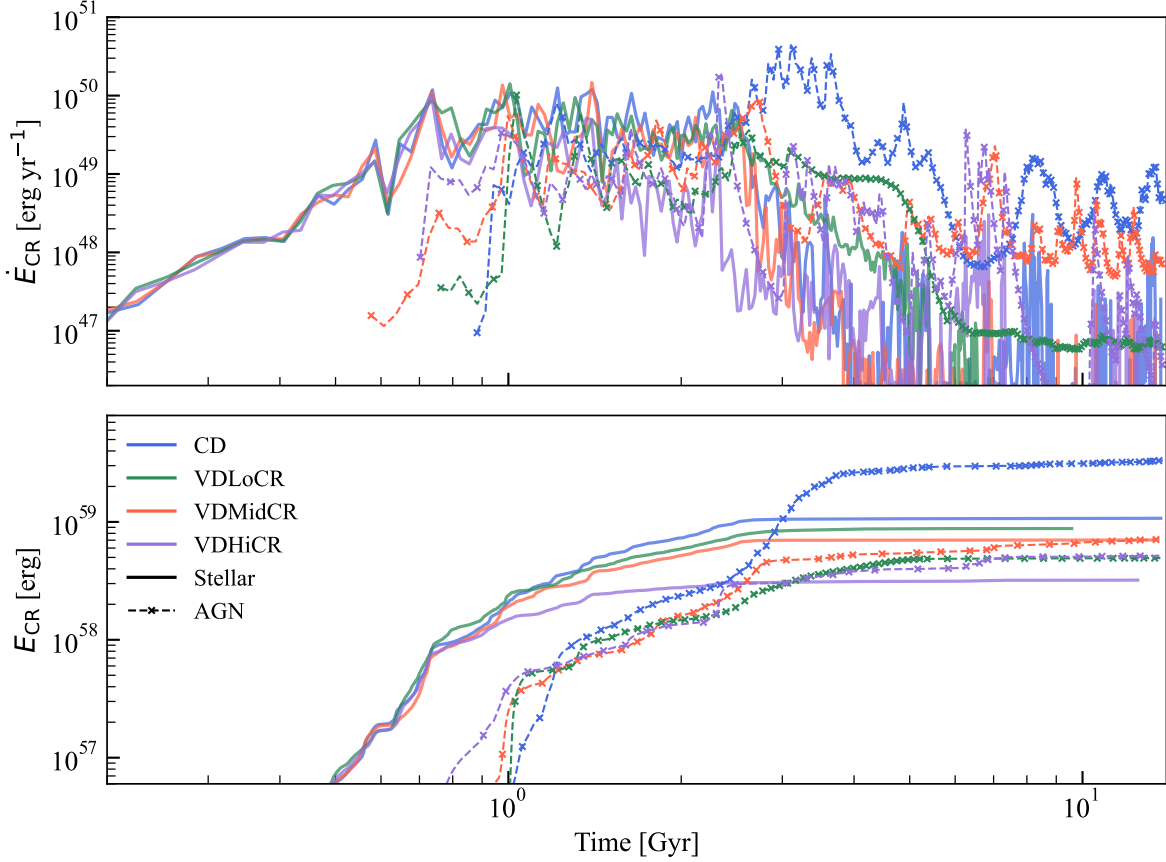
Figure 5. Cosmic ray injection rate (top) and cumulative injected energy (bottom) by source of the `h206` runs, from 0 to 13.8 Gyr. Stellar feedback is plotted in solid; AGN feedback is plotted in dashed lines with 'x' markers. The injection rate is binned at ~30 Myr intervals for both stellar and AGN injection. Stellar injection rate is relatively steady-state after ~6 Gyr with respect to star-forming galaxies. All runs exhibit a moving average in AGN injection rate. VDMidCR has the earliest AGN-projected CR injection and has both the highest injection rate and cumulative injection at 13.8 Gyr compared to the other VD runs. Unlike other runs, VDLoCR's AGN injection rate stabilizes beyond ~6 Gyr.

The VDMidCR and VDHiCR runs have slightly earlier initial AGN injection times and exhibit higher variation in AGN injection rates at late times, but still on average lower than that of the CD model. As expected, stellar CR injection rates are relatively low compared to star-forming galaxies after quenching past ~6 Gyr, with brief bursts typically sub-dominant to the BH contribution. This indicates all models primarily regulate via AGN feedback, and more so that they are regulated via its responsiveness, here particularly that of the CR feedback model (Wellons et al. 2023).

Sam: TODO: We should add some discussion here regarding the connection to 'quasar-mode' and 'radio-mode' feedback (and 'feedback-regulated' or 'fueling-regulated' black-hole growth in connection to the M-sigma, Mstar-Mhalo, and CR energy density profiles. added some relevant citations to the .bib file). some rough text below

We note here also that the self-regulation our simulated galaxies exhibit is non-trivial. In Fig. 3.1, we showed that for increasing CR feedback efficiency, `h206` runs *moved down* the $z = 0$ SMHM relation while moving *along* the M_{BH}-σ relation. In the feedback-regulated BH growth picture (Di Matteo et al. 2005; Sijacki et al. 2007, 2009), accretion onto the BH gets shut down due to 'quasar-mode' feedback, which is more ejective & explosive in nature. This is evinced by the linear relationship of the inner e_{CR} profiles' normalizations at early times in Fig. 2, which are tracing the injection of CRs near the peak of BH growth. M_{BH} is then set inversely to ϵ_{CR} at fixed σ, which is set by the assembly history of the halo at early times.

Subsequently, evolution enters a 'fueling-regulated' mode (commonly referred to or implemented as 'radio-mode' feedback; Weinberger et al. 2018) where M_{BH} changes slowly and star-formation is modulated by pre-

vention of gas accretion. This 'maintenance-mode' allows for M_* to change, modifying the central potential and thus σ, moving points down the SMHM relation and along the M_{BH}-σ relation.

Importantly, in our simulations here, we have not inserted 'by hand' any qualitative change in the feedback prescription for varied Eddington ratios as in large-volume cosmological simulations – the halos' collective response to feedback naturally arises from the coupling of feedback to gas, which varies in its responsiveness, and the cosmological assembly of the galaxies. This highlights how multi-channel AGN feedback, varied solely in CR efficiency, can naturally produce *both* qualitative feedback behaviors necessary to reproduce bulk massive galaxy observables.

4. DISCUSSION AND CONCLUSIONS

In this work, we have explored plausible models for AGN feedback with varied CR injection efficiencies from the black hole, and two different CR transport models. All parameterizations of CR physics explored here produce reasonable, quenched galaxies, suggesting that bulk properties of the galaxies are relatively insensitive to CR parameterizations. However, the radial profiles of CR energy density and gas properties reveal differences in model predictions, which may reveal an avenue to constrain how AGN feedback regulates galaxies, and particularly, the role of CRs in quenching.

The CR energy density profiles are flatter than expected from a constant injection of CRs and steady-state halo CR pressure (Butsky et al. 2023), which owes to the time-dependent nature of the injection. Ponnada (2025) show that time-dependent injection of CRs (decreasing $\dot{E}_{CR}$ with time) undergoing a mix of diffusive- and streaming/advection-like transport leads to flattening of $P_{CR}(r)$ relative to time-steady expectations.

Indeed, therein this behavior for the same CD run of `m13h206` we analyze here is shown and agrees well with time-dependent analytic expectations. The CGM n_{gas} profiles also appear to flatten similarly, which may indicate that the CRs are playing a role in driving outflows via their dynamical coupling to the gas.

In Figure 5, we detailed the fine-grained CR injection rates from AGN and star-formation for each `h206` run. These largely show a decreasing $\langle \dot{E}_{CR} \rangle$ with time, where $\langle \rangle$ denotes averaging over some effective transport timescale out to CGM radii. However, there is significant burstiness on short timescales, which depending on the balance of diffusive- vs. streaming/advection-like transport will be "smeared out" to varying degrees.

Our current understanding of CR transport physics, which is critical for modulating CGM phase structure,

is limited by the lack of direct observables that track CRs and low-density CGM. Moreover, ϵ_{CR}^{BH} is a highly uncertain quantity, and may also vary in terms of hadronic/leptonic composition (Lin et al. 2023). FIRE-2 simulations evolved with single-bin treatments of CRs with different physically-motivated sub-grid scattering prescriptions have produced varying CGM properties (Ponnada et al. 2024; Hopkins et al. 2020a), as have FIRE-3 galaxies evolved with AGN feedback and varied multi-bin CR transport physics (including some explored herein), specifically differing in morphological evolution of the far-infrared-radio correlation (Ponnada et al. 2025b), which may be independently constraining for CR effects in the ISM and inner CGM when compared to spatially resolved observations (Murphy et al. 2006).

Recently, (Hopkins et al. 2025) proposed inverse Compton emission from CR leptons as a method by which to estimate the CR lepton pressure, which is largely tracing the AGN-produced CRs for these simulations at late times (at least within $\sim 1 - 2\,R_{vir}$ for the κ_{eff} modeled here). The distinctions between the n_{gas} and P_{CR} profiles for different ϵ_{CR}^{BH} (for a fixed CR transport model) appear promising towards constraining ϵ_{CR}^{BH}, but a more statistical sample of simulations and corresponding synthetic observations would be needed to compare against existing constraints, which are often stacked measurements (e.g., from eROSITA Zhang et al. 2024a,b, 2025).

There is also the complementary probe of thermal pressure in the CGM via the thermal Sunyaev-Zel'dovich effect, which when combined with X-ray constraints may be particularly constraining how CRs contribute to galaxy quenching (Ponnada et al. 2025a). Quenched massive galaxies appear to be brigher than their star-forming counterparts with the latest detections (Zhang et al. 2025), while simulations invoking AGN feedback without CRs tend to over-predict the detected halo-integrated tSZ signal by over an order–of–magnitude (Das et al. 2025).

So, by producing synthetic synchrotron (Ponnada et al. 2023), IR-O/UV (Byrne et al. 2024; Wijers et al. 2024; Qutob et al. 2024; Ponnada et al. 2025b), and X-ray predictions (Chadayammuri et al. 2022; Lu et al. 2025) for feedback parameterized with varied CR injection efficiencies and transport parameterizations, our results suggest we may be able to constrain these physics via observational comparisons of spectrally-resolved CR-MHD simulations with explicit evolution of multi-channel AGN feedback. While the AGN feedback schemes explored herein have injected the multi-channel feedback energy and momentum on the accretion-kernel

scale ($\sim 1 - 10\,\mathrm{pc}$ from the central source), recent developments using idealized setups have suggested that alternative modes of CR injection, e.g. at jet termination shocks (Su et al. 2025), may qualitatively change the quenching and maintenance behavior of a fixed set of feedback parameters in massive galaxies. Our results motivate further exploring such models with explicit feedback in cosmological runs.

Finally, we note that structures we see arising in $P_{CR}(r)$ due to time-dependence as well as variation in κ_{eff} at large radii may potentially connect to formation of Odd Radio Circles (ORCs) observed in radio surveys around massive galaxies (Norris et al. 2021). Since we

have only explored one plausible model for spatially variable CR scattering, we do not perform a comprehensive comparison here, and leave it to future work.

REFERENCES

Astropy Collaboration, Robitaille, T. P., Tollerud, E. J., et al. 2013, A&A, 558, A33, doi: 10.1051/0004-6361/201322068

Behroozi, P., Wechsler, R. H., Hearin, A. P., & Conroy, C. 2019, Monthly Notices of the Royal Astronomical Society, 488, 3143, doi: 10.1093/mnras/stz1182

Benson, A. J. 2010, Galaxy formation theory, Elsevier BV, doi: 10.1016/j.physrep.2010.06.001

Berezinsky, V., Gazizov, A., & Grigorieva, S. 2006, Physical Review D, 74, doi: 10.1103/physrevd.74.043005

Bustard, C., & Zweibel, E. G. 2021, The Astrophysical Journal, 913, 106, doi: 10.3847/1538-4357/abf64c

Butsky, I. S., Nakum, S., Ponnada, S. B., et al. 2023, Monthly Notices of the Royal Astronomical Society, 521, 2477, doi: 10.1093/mnras/stad671

Butsky, I. S., & Quinn, T. R. 2018, The Astrophysical Journal, 868, 108, doi: 10.3847/1538-4357/aaeac2

Byrne, L., Faucher-Giguère, C.-A., Wellons, S., et al. 2024, The Astrophysical Journal, 973, 149, doi: 10.3847/1538-4357/ad67ca

Chadayammuri, U., Bogdan, A., Oppenheimer, B. D., et al. 2022, The Astrophysical Journal Letters, 936, L15, doi: 10.3847/2041-8213/ac8936

Cole, S., Lacey, C. G., Baugh, C. M., & Frenk, C. S. 2002, Monthly Notices of the Royal Astronomical Society, 319, 168, doi: 10.1046/j.1365-8711.2000.03879.x

Das, S., Truong, N., Chiang, Y.-K., & Mathur, S. 2025, The Astrophysical Journal, 991, 205, doi: 10.3847/1538-4357/adfdd6

Davé, R., Anglés-Alcázar, D., Narayanan, D., et al. 2019, Monthly Notices of the Royal Astronomical Society, 486, 2827–2849, doi: 10.1093/mnras/stz937

Di Matteo, T., Springel, V., & Hernquist, L. 2005, Nature, 433, 604, doi: 10.1038/nature03335

Fabian, A. C. 2012, Annual Review of Astronomy and Astrophysics, 50, 455, doi: 10.1146/annurev-astro-081811-125521

Greene, J. E., Strader, J., & Ho, L. C. 2020, Annual Review of Astronomy and Astrophysics, 58, 257, doi: 10.1146/annurev-astro-032620-021835

Harrison, C. M., & Almeida, C. R. 2024, Observational Tests of Active Galactic Nuclei Feedback: An Overview of Approaches and Interpretation, arXiv. http://arxiv.org/abs/2404.08050

Harrison, C. M., Costa, T., Tadhunter, C. N., et al. 2018, Nature Astronomy, 2, 198, doi: 10.1038/s41550-018-0403-6

Heckman, T. M., & Best, P. N. 2014, Annual Review of Astronomy and Astrophysics, 52, 589, doi: 10.1146/annurev-astro-081913-035722

Hopkins, P. F. 2015, Monthly Notices of the Royal Astronomical Society, 450, 53, doi: 10.1093/mnras/stv195

Hopkins, P. F., Butsky, I. S., Panopoulou, G. V., et al. 2022a, Monthly Notices of the Royal Astronomical Society, 516, 3470, doi: 10.1093/mnras/stac1791

Hopkins, P. F., Chan, T. K., Ji, S., et al. 2021, Monthly Notices of the Royal Astronomical Society, 501, 3640, doi: 10.1093/mnras/staa3690

Hopkins, P. F., Chan, T. K., Squire, J., et al. 2020a, Monthly Notices of the Royal Astronomical Society, 501, 3663, doi: 10.1093/mnras/staa3692

Hopkins, P. F., Quataert, E., Ponnada, S. B., & Silich, E. 2025, The Open Journal of Astrophysics, 8, 78, doi: 10.33232/001c.141293

Hopkins, P. F., & Raives, M. J. 2015, Monthly Notices of the Royal Astronomical Society, 455, 51, doi: 10.1093/mnras/stv2180

Hopkins, P. F., Squire, J., Butsky, I. S., & Ji, S. 2022b, Monthly Notices of the Royal Astronomical Society, doi: 10.1093/mnras/stac2909

Hopkins, P. F., Torrey, P., Faucher-Giguère, C.-A., Quataert, E., & Murray, N. 2016, Monthly Notices of the Royal Astronomical Society, 458, 816, doi: 10.1093/mnras/stw289

Hopkins, P. F., Wetzel, A., Kereš, D., et al. 2018, Monthly Notices of the Royal Astronomical Society, 480, 800, doi: 10.1093/mnras/sty1690

Hopkins, P. F., Chan, T. K., Garrison-Kimmel, S., et al. 2020b, Monthly Notices of the Royal Astronomical Society, 3465, doi: 10.1093/mnras/stz3321

Hopkins, P. F., Wetzel, A., Wheeler, C., et al. 2023, Monthly Notices of the Royal Astronomical Society, 519, 3154, doi: 10.1093/mnras/stac3489

Jokipii, J. R. 1966, The Astrophysical Journal, 146, 480, doi: 10.1086/148912

Kereš, D., Katz, N., Davé, R., Fardal, M., & Weinberg, D. H. 2009, Monthly Notices of the Royal Astronomical Society, 396, 2332–2344, doi: 10.1111/j.1365-2966.2009.14924.x

Lin, Y.-H., Yang, H.-Y. K., & Owen, E. R. 2023, Monthly Notices of the Royal Astronomical Society, 520, 963, doi: 10.1093/mnras/stad185

Longair, M. S. 2008, Galaxy Formation, Astronomy and Astrophysics Library (Heidelberg, Germany: Springer), doi: 10.1007/978-3-540-73478-9

Lu, Y. S., Kereš, D., Hopkins, P. F., et al. 2025, Constraining cosmic ray transport models using circumgalactic medium properties and observables, arXiv, doi: 10.48550/arXiv.2505.13597

Murphy, E. J., Braun, R., Helou, G., et al. 2006, The Astrophysical Journal, 638, 157–175, doi: 10.1086/498636

Norris, R. P., Crawford, E., & Macgregor, P. 2021, Galaxies, 9, 83, doi: 10.3390/galaxies9040083

Ponnada, S. B. 2025, Time-Dependent Cosmic Ray Halos from Bursty Star Formation and Active Galactic Nuclei: Semi-Analytic Formalism and Galaxy Formation Implications, arXiv, doi: 10.48550/arXiv.2509.02697

Ponnada, S. B., Hopkins, P. F., Lu, Y. S., et al. 2025a, Strong Evidence for Cosmic Ray-Supported $\sim L^{\ast}$ Galaxy Halos via X-ray & tSZ Constraints, arXiv, doi: 10.48550/arXiv.2510.13959

Ponnada, S. B., Panopoulou, G. V., Butsky, I. S., et al. 2023, Monthly Notices of the Royal Astronomical Society, 527, 11707–11718, doi: 10.1093/mnras/stad3978

Ponnada, S. B., Butsky, I. S., Skalidis, R., et al. 2024, Synchrotron Signatures of Cosmic Ray Transport Physics in Galaxies. https://arxiv.org/abs/2309.16752

Ponnada, S. B., Cochrane, R. K., Hopkins, P. F., et al. 2025b, The Astrophysical Journal, 980, 135, doi: 10.3847/1538-4357/ada280

Qutob, N., Emami, R., Su, K.-Y., et al. 2024, The Astrophysical Journal, 977, 72, doi: 10.3847/1538-4357/ad8658

Ruszkowski, M., Yang, H.-Y. K., & Reynolds, C. S. 2017, The Astrophysical Journal, 844, 13, doi: 10.3847/1538-4357/aa79f8

Salim, S., Rich, R. M., Charlot, S., et al. 2007, The Astrophysical Journal Supplement Series, 173, 267, doi: 10.1086/519218

Schaye, J., Crain, R. A., Bower, R. G., et al. 2014, Monthly Notices of the Royal Astronomical Society, 446, 521–554, doi: 10.1093/mnras/stu2058

Sijacki, D., Springel, V., Di Matteo, T., & Hernquist, L. 2007, Monthly Notices of the Royal Astronomical Society, 380, 877, doi: 10.1111/j.1365-2966.2007.12153.x

Sijacki, D., Springel, V., & Haehnelt, M. G. 2009, Monthly Notices of the Royal Astronomical Society, 400, 100, doi: 10.1111/j.1365-2966.2009.15452.x

Sijacki, D., Vogelsberger, M., Genel, S., et al. 2015, Monthly Notices of the Royal Astronomical Society, 452, 575–596, doi: 10.1093/mnras/stv1340

Somerville, R. S., & Davé, R. 2015, Annual Review of Astronomy and Astrophysics, 53, 51, doi: 10.1146/annurev-astro-082812-140951

Springel, V., & Hernquist, L. 2003, Monthly Notices of the Royal Astronomical Society, 339, 312, doi: 10.1046/j.1365-8711.2003.06207.x

Su, K.-Y., Bryan, G. L., Hopkins, P. F., et al. 2025, Modeling Cosmic Rays at AGN Jet-Driven Shock Fronts, arXiv, doi: 10.48550/arXiv.2502.00927

Su, K.-Y., Hopkins, P. F., Hayward, C. C., et al. 2019a, Monthly Notices of the Royal Astronomical Society, 487, 4393, doi: 10.1093/mnras/stz1494

—. 2019b, Cosmic rays or turbulence can suppress cooling flows (where thermal heating or momentum injection fail), Oxford University Press (OUP), doi: 10.1093/mnras/stz3011

Su, K.-Y., Hopkins, P. F., Bryan, G. L., et al. 2021, Monthly Notices of the Royal Astronomical Society, 507, 175, doi: 10.1093/mnras/stab2021

Weinberger, R., Springel, V., Pakmor, R., et al. 2018, Monthly Notices of the Royal Astronomical Society, 479, 4056, doi: 10.1093/mnras/sty1733

Wellons, S., Faucher-Giguère, C.-A., Hopkins, P. F., et al. 2023, Monthly Notices of the Royal Astronomical Society, 520, 5394, doi: 10.1093/mnras/stad511

Wijers, N. A., Faucher-Giguère, C.-A., Stern, J., Byrne, L., & Sultan, I. 2024, The Astrophysical Journal, 973, 99, doi: 10.3847/1538-4357/ad63a0

Zhang, Y., Comparat, J., Ponti, G., et al. 2024a, Astronomy & Astrophysics, 690, A267, doi: 10.1051/0004-6361/202449412

—. 2024b, Astronomy & Astrophysics, 690, A268, doi: 10.1051/0004-6361/202449413

—. 2025, Astronomy & Astrophysics, 693, A197, doi: 10.1051/0004-6361/202452273